Journal of ELECTRONIC MATERIALS, Vol. 45, No. 7, 2016
DOI: 10.1007/s11664-016-4504-7

Effect of Reflow Time on Wetting Behavior, Microstructure Evolution, and Joint Strength of Sn-2.5Ag-0.5Cu Solder on Bare and Nickel-Coated Copper Substrates

MRUNALI SONA[1] and K. NARAYAN PRABHU[1,2]

1.—Department of Metallurgical & Materials Engineering, National Institute of Technology Karnataka, Surathkal, Mangalore 575 025, India. 2.—e-mail: prabhukn_2002@yahoo.co.in

The effect of reflow time on wetting behavior of Sn-2.5Ag-0.5Cu lead-free solder on bare and nickel-coated copper substrates has been investigated. The solder alloy was reflowed at 270°C for various reflow times of 10 s, 100 s, 300 s, and 500 s. On bare copper substrate, the intermetallic compound (IMC) thickness increased with increase in reflow time, whereas on Ni-coated Cu substrate, the IMC thickness increased up to 300 s followed by a drop for solder alloy reflowed for 500 s. The spreading behavior of the solder alloy was categorized into capillary, gravity (diffusion), and viscous zones. Gravity zone was obtained from 3.8 ± 0.43 s to 38.97 ± 3.38 s and from 5.99 ± 0.5 s to 77.82 ± 8.84 s for the Sn-2.5Ag-0.5Cu/Cu and Sn-2.5Ag-0.5Cu/Ni/Cu system, respectively. Sn-2.5Ag-0.5Cu solder alloy was also reflowed for the period corresponding to the end of the gravity zone (40 s and 80 s on bare and Ni-coated Cu, respectively). The joint strength was maximum at reflow time of 40 s and 80 s for the Sn-2.5Ag-0.5Cu/Cu and Sn-2.5Ag-0.5Cu/Ni/Cu system, respectively. The dynamic contact angle at the end of the gravity (diffusion) zone (θ_{gz}) was found to be a better parameter compared with the stabilized contact angle (θ_f) to assess the effect of the wettability of the liquid solder on the microstructure and joint strength. The present investigation reveals the significance of the gravity zone in assessment of optimum reflow time for lead-free solder alloys.

Key words: Sn-Ag-Cu (SAC) solder, contact angle, wettability, IMC, joint shear strength

INTRODUCTION

Lead–tin solder alloys are used in electronic assemblies owing to their low cost and good performance. However, use of lead-bearing solders is banned in many countries due to the inherent toxicity of lead and adverse environmental and health risks associated with it. Tin-rich, binary or ternary alloys are being actively studied as alternative, lead-free solders. Several elements such as Bi, Ag, Cu, In, Sb, and Zn have been used as alloying additions.[1,2] Currently, Sn-Ag-Cu (SAC) ternary alloys are being considered as replacements for conventional Pb-Sn solders because of their good thermal stability and excellent mechanical properties. However, relatively high melting temperature, poor wettability, and fast reaction rate with metallization layer are drawbacks of SAC solders.[3] It is well established that wetting plays a major role in the formation of a metallurgical bond at the solder–substrate interface, describing the extent of intimate contact between a liquid and solid.[4] The extent of wetting is measured by the contact angle formed at the triple point between the three phases, namely solid, liquid, and vapor, and the substrate surface.[5] The rate of wetting indicates how quickly the liquid wets and spreads over the surface. The thermal conditions of the system, the viscosity of the liquid, and chemical reactions occurring at the interface

(Received September 7, 2015; accepted March 29, 2016; published online April 12, 2016)

are the major factors affecting spreading of liquid solder on solid substrate.[4] Chemical reactions at the interface result in formation of intermetallic compounds (IMCs). This intermetallic layer is a critical part of a solder joint, because it facilitates bonding between the solder and substrate. At low levels, such compounds have a strengthening effect on the joint, but at higher levels, they tend to make solder joints more brittle.[6] Hence, it is vital to understand the sequence of IMC formation and growth during soldering, as the thickness and morphology of the IMC layer impact on solder joint strength.[7]

Copper is the substrate most widely used in microelectronic devices due to its high corrosion resistance, good wettability, good solderability, and high thermal conductivity. However, quick oxidation of Cu when exposed to environmental conditions results in reduced wettability and solderability. Surface finish is therefore generally used to protect copper from oxidation, contamination, and mishandling prior to assembly. A few common surface finishes are immersion gold over electroless or electrolytic nickel (ENIG), immersion tin (ImSn), immersion silver (ImAg), organic solderability preservative (OSP), and lead-free (SAC or Sn-Cu) hot-air solder leveling (HASL).[8–11] Choubey et al.[11] studied intermetallic growth during solid-state aging at 100°C and 125°C up to 1000 h for Sn-3.5Ag and Sn-3.0Ag-0.5Cu solder alloys on various pad finishes such as ImSn, ImAg, OSP, and ENIG. Sn-3.5Ag solder on ENIG pad finish showed a significantly thinner IMC layer compared with ImSn, ImAg, and OSP pad finishes, whereas comparable IMC thickness was observed for Sn-3.0Ag-0.5Cu solder on various surface finishes. Aging at higher temperature resulted in thicker IMC for all solder–substrate systems investigated. Ni acts as a diffusion barrier layer for Cu/Sn-based solders in electronics, since the reaction rate of Ni with Sn is typically several orders of magnitude lower than that of Cu with Sn.[12,13] Use of Ni has been associated with improvement in solidification microstructures, increased volume fraction of eutectic phase, and lower propensity for interfacial IMCs to crack during service.[14] Though ENIG is suggested for long-term applications, it is prone to black pad, which forms during the plating process and can lead to early failure. Black pad is associated with the phosphorus content in the electroless-nickel coating bath. During the electroless process, a few atomic percent of phosphorus is codeposited with Ni. This presence of P with Ni complicates the chemical reactions between Ni and solder. High phosphorus content gives good corrosion resistance but induces solder joint embrittlement with growth of an intermetallic layer through phosphorus enrichment during soldering. Low phosphorus content in the electroless-nickel coating results in poor corrosion resistance.[15] Islam et al.[16] investigated the dissolution kinetics of electrolytic Ni and electroless NiP metallization for Sn-3.5Ag-0.5Cu solder reflowed at 250°C. All samples in as-reflowed state were kept again at 250°C for 5 min, 10 min, 30 min, 120 min, and 180 min. From the results of this experiment, it was concluded that a P-rich nickel layer can act as a diffusion barrier and decrease the IMC growth rate compared with electrolytic Ni. However, this weakens the interface and reduces the ball shear strength and reliability. You et al.[17] studied the reliability of eutectic Sn-Pb, Sn-1.0Ag-0.5Cu, Sn-3.0Ag-0.5Cu, and Sn-4.0Ag-0.5Cu solder alloys on three different pad surface finishes (ENIG, electrolytic Ni/Au, and OSP). The results showed that electrolytic Ni/Au surface finish had the highest fracture force for all three SAC solder alloys, whereas the average fracture force of the Sn-Pb solder joint was independent of the type of surface finish. Among the SAC solder alloys, Sn-1.0Ag-0.5Cu and Sn-3.0Ag-0.5Cu showed comparable fracture force on Ni-Au surface finish. Use of gold coating over electroless or electrolytic Ni to protect it from oxidation may degrade the mechanical properties of the solder joint. Due to the high dissolution rate and solubility of Au in molten solder, the entire Au layer disappears from the joint interface after a typical reflow process, and a large number of $(Au_xNi_{1-x})Sn_4$ particles form inside the bulk solder. During solid-state annealing, regrouping of $(Au_xNi_{1-x})Sn_4$ at the solder–substrate interface takes place, which in turn reduces the mechanical properties of the joint.[18]

Most previous research work on lead-free solders has focused solely on the effect of reflow time on interfacial microstructure. Few studies have investigated its effect on both the interfacial microstructure and resulting joint strength. There is no clear understanding of the effect of reflow time on wettability of solder alloy on the substrate. In all previous research, wettability was assessed by measuring the equilibrium contact angle. It is well known that interfacial reactions take place immediately when liquid metal contacts the substrate. Hence, a correlation between the equilibrium contact angle and joint strength may be misleading, particularly in the case of reactive systems; Under such circumstances, spreading kinetics has to be taken into account. Therefore, the present work focused on study of the wetting kinetics of Sn-2.5Ag-0.5Cu on bare and Ni-coated Cu substrates, the interfacial reaction at the solder–substrate interface, and the corresponding joint strength as a function of reflow time, using a novel quench setup to obtain precise control over reflow time.

EXPERIMENTAL PROCEDURES

Sn-2.5Ag-0.5Cu solder alloy was procured in wire form (Ø0.8 mm) from Antex Electronics Ltd., UK. The solder wire was melted to prepare spherical solder balls of 0.080 g weight using a solder

station (Ersa Digital 2000 A). Cu substrates (Ø12 mm × 8 mm) were polished using SiC papers of varying grit size (1/0 to 4/0 grade) followed by velvet cloth disk polishing using diamond lapping compound to obtain smooth surface finish. An equal number of Cu substrates were electroplated with Ni. The thickness of the Ni layer electroplated on top of the Cu substrate was about 15 μm. Surface profiles of the substrates were measured using a Form Talysurf 50 surface profiler; The arithmetic-mean roughness (R_a) values were in the range of 0.01 ± 0.006 μm and 0.04 ± 0.008 μm for bare and Ni-coated Cu substrates, respectively. Contact angle measurements were carried out using an FTA 200 dynamic contact angle analyzer; This equipment has a flexible video system for measuring contact angle. Spherical balls of solder alloy (average diameter 2.76 ± 0.035 mm) were placed on the substrate, after coating the substrate surface with flux (inorganic acid, Alfa Aesar, USA). The solder–substrate system was then kept inside an environmental chamber maintained at reflow temperature of 270°C throughout the experiment. The spreading process was recorded and the captured images were analyzed using FTA software (FTA 32 Video 2.0) to determine the wetting behavior of the solder. A quench cooling method was adopted to cool the sample at a desired reflow time. Figure 1 shows a schematic of the quench cooling setup, consisting of a steel rod with a specimen holder. The steel rod was suspended in a vertical tubular furnace after the specimen holder was loaded with the solder–substrate system. The vertical tubular furnace was maintained at reflow temperature of 270°C throughout the experiment. Reflow time was counted as the solder started spreading. At the end of reflow time, the steel rod was released and the solder–substrate system quenched in water kept in a 2-L beaker just below the furnace. A Zeiss stereomicroscope (Stemi 2000-C) was used to obtain macroimages of the solder sessile drop after spreading. The solder drop bonded to the substrate was sectioned along the axis and polished using SiC paper of 1/0, 2/0, 3/0, and 4/0 grade followed by velvet cloth disk polishing using colloidal silica polishing suspension. The polished samples were then etched with 5% Nital for about 3 s to 5 s. The solder–substrate interfacial region was examined by scanning electron microscopy (SEM, JEOL JSM 6380LA) combined with energy-dispersive spectroscopy (EDS) to study the reaction between the alloy and solid substrate and the possible formation of different compounds at the interface. Shear testing was performed on solder droplet samples using a Nordson DAGE 4000Plus bond tester. The height of the shear tool and the shear speed were chosen as 1 μm and 200 μm/s, respectively. Force–displacement curves were recorded during the shear test. After the ball shear test, the failure mode was assessed by examining the fractured surface under scanning electron microscope.

RESULTS AND DISCUSSION

Wetting Behavior

Figure 2 shows a schematic of the dynamic contact angle analyzer. Typical relaxation curves showing various regimes involved during the spreading of Sn-2.5Ag-0.5Cu on bare and Ni-coated Cu substrates are shown in Fig. 3a and b, respectively. Various regimes were recognized by a sharp change in spreading rate in the relaxation curve. Regimes involved during solder spreading were identified by the change of slope in plots of θ versus T, where θ is the contact angle (°) during spreading and T is time (s). The spreading behavior showed continuous change in the contact angle and base radius (drop base area) of the solder alloy with time. Figure 4a and b present the variation of the base radius with time for the solder on bare and Ni-coated Cu substrate, respectively. In an ideal condition, the entire base diameter versus time curves should lie on top of each other, but a discrepancy was observed, which can be attributed to slight variation

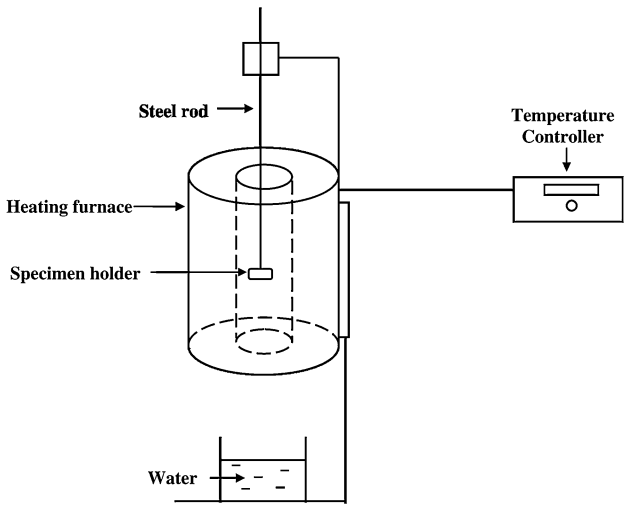

Fig. 1. Schematic of quench cooling setup.

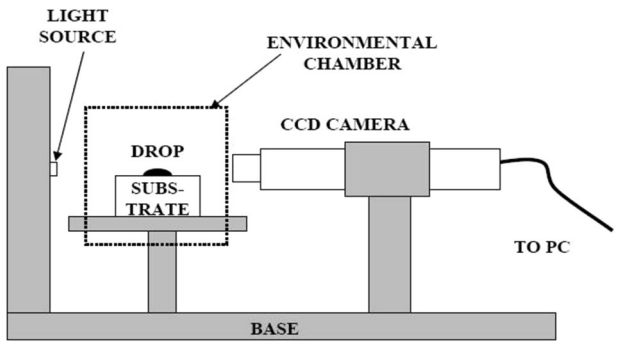

Fig. 2. Schematic of dynamic contact angle analyzer.

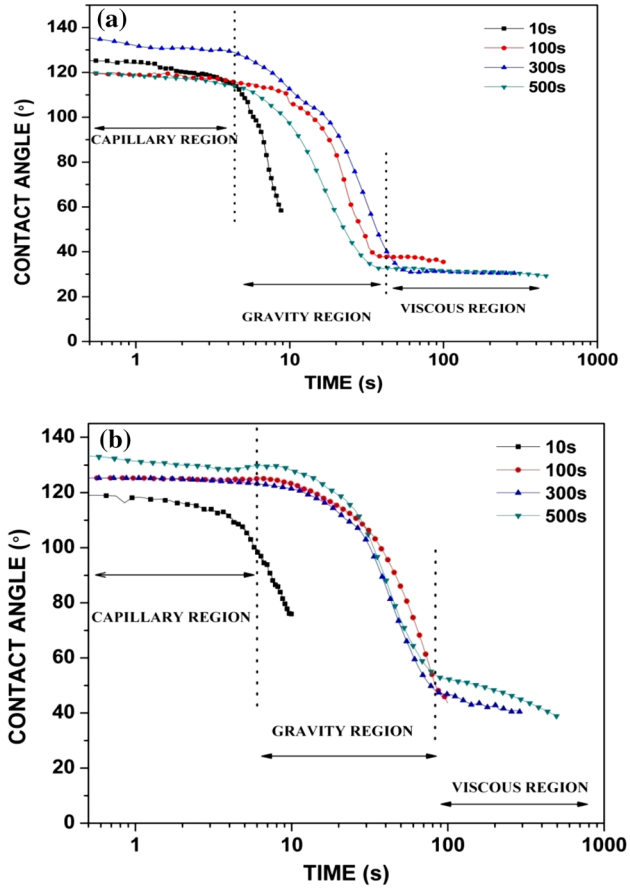

Fig. 3. Relaxation curves for Sn-2.5Ag-0.5Cu on (a) bare and (b) Ni-coated Cu substrate.

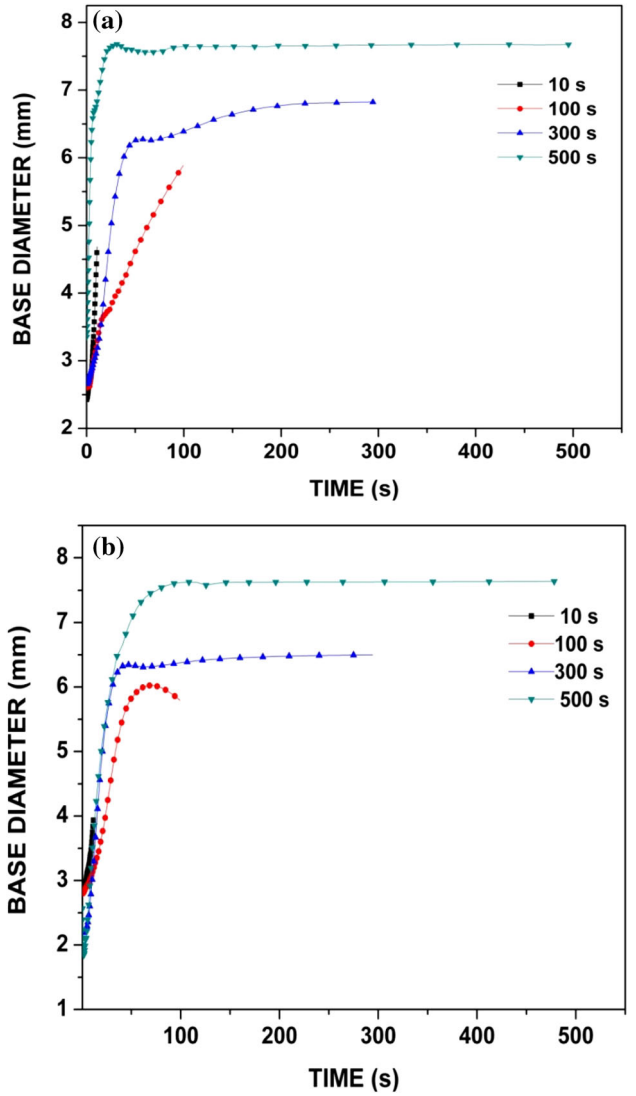

Fig. 4. Variation of solder alloy base radius with time when reflowed on (a) bare and (b) Ni-coated Cu substrate for various reflow times.

in substrate surface roughness and solder ball mass and diameter due to experimental limitations. Spreading of the molten solder in the radial direction was observed. After solidification, all specimens exhibited spherical cap shape. The three regimes involved during spreading of Sn-2.5Ag-0.5Cu on bare and Ni-coated Cu substrate were capillary, gravity (reactive), and viscous zones. The duration of the capillary zone and gravity zone during reflow of the solder alloy on bare and Ni-coated Cu substrates reflowed for various reflow times are presented in Table I. The period of the capillary zone was about 3.8 ± 0.43 s and 5.99 ± 0.5 s for the Sn-2.5Ag-0.5Cu/Cu and Sn-2.5Ag-0.5Cu/Ni/Cu system, respectively. The gravity zone was found from 3.8 ± 0.43 s to 38.97 ± 3.38 s and from 5.99 ± 0.5 s to 77.82 ± 8.84 s for the Sn-2.5Ag-0.5Cu/Cu and Sn-2.5Ag-0.5Cu/Ni/Cu system, respectively. The contact angle of the solder drops abruptly in the capillary and gravity zones compared with the viscous zone. In the capillary zone, physical spreading of the molten solder takes place by capillary action due to reduction in surface tension. Spreading in this regime is similar to nonreactive spreading of any liquid on a solid substrate surface. Diffusion and chemical reactions take place at the solder–substrate interface in the gravity zone, and the molten solder completely contacts the substrate surface. A metallurgical contact between the solder and substrate forms in the gravity zone due to dissolution of the substrate into the molten solder. Solid IMC starts to form at the interface at the local equilibrium solubility.[19] Therefore, the spreading of molten solder in the gravity region is reactive. The period of the gravity zone for the Sn-2.5Ag-0.5Cu/Ni/Cu system was found to be twice that for the Sn-2.5Ag-0.5Cu/Cu system. This shows that Ni acts as a barrier to solder–substrate interfacial reaction. Spreading of liquid solder more or less stops in the viscous region. Sn-2.5Ag-0.5Cu solder alloy was therefore reflowed on bare and Ni-coated Cu substrates for 40 s and 80 s, respectively, being the approximate times beyond which the reactive (gravity) zone ends. Average relaxation rates in the capillary, gravity, and viscous zones for the

Table I. Duration of capillary and gravity regimes for solder alloy on bare and Ni-coated Cu substrate surfaces

	Sn-2.5Ag-0.5Cu/Cu				Sn-2.5Ag-0.5Cu/Ni/Cu			
Reflow time (s)	Period of capillary regime (s)	Contact angle at end of capillary regime, θ_{cz} (°)	Period of gravity regime (s)	Contact angle at end of gravity regime, θ_{gz} (°)	Period of capillary regime (s)	Contact angle at end of capillary regime, θ_{cz} (°)	Period of gravity regime (s)	Contact angle at end of gravity regime (θ_{gz}) (°)
10	4.18	115.11	–	–	5.25	104.81	–	–
100	3.21	117.33	3.21–36.34	39.32	6.28	125.10	6.28–75.46	57.48
300	3.78	129	3.78–42.79	40.12	5.99	123.28	5.99–87.61	47.54
500	4.05	114.35	4.05–37.80	32.94	6.45	129.72	6.45–70.40	58.98

Table II. Effect of reflow time on wetting behavior and interfacial reaction of Sn-2.5Ag-0.5Cu/Cu and Sn-2.5Ag-0.5Cu/Ni/Cu solder joints

	Sn-2.5Ag-0.5Cu/Cu				Sn-2.5Ag-0.5Cu/Ni/Cu		
Reflow time (s)	Stabilized contact angle, θ_f (°)	IMC formed	IMC thickness (μm)	Reflow time (s)	Stabilized contact angle, θ_f (°)	IMC formed	IMC thickness (μm)
10	43.72 ± 3.48	Cu_6Sn_5	0.75	10	56.43 ± 2.20	$(CuNi)_6Sn_5$	0.69
40	36.93 ± 1.17	Cu_6Sn_5	1.04	80	44.52 ± 2.71	$(CuNi)_6Sn_5$	0.84
100	35.88 ± 1.02	Cu_6Sn_5	1.197	100	42.69 ± 1.24	$(CuNi)_6Sn_5$	1.81
300	31.25 ± 1.78	Cu_6Sn_5	1.81	300	40.78 ± 0.52	$(CuNi)_6Sn_5$	2.86
500	29.26 ± 1.35	Cu_6Sn_5	1.95	500	37.73 ± 0.40	$(CuNi)_6Sn_5$ $(CuNi)_3Sn_4$	1.99

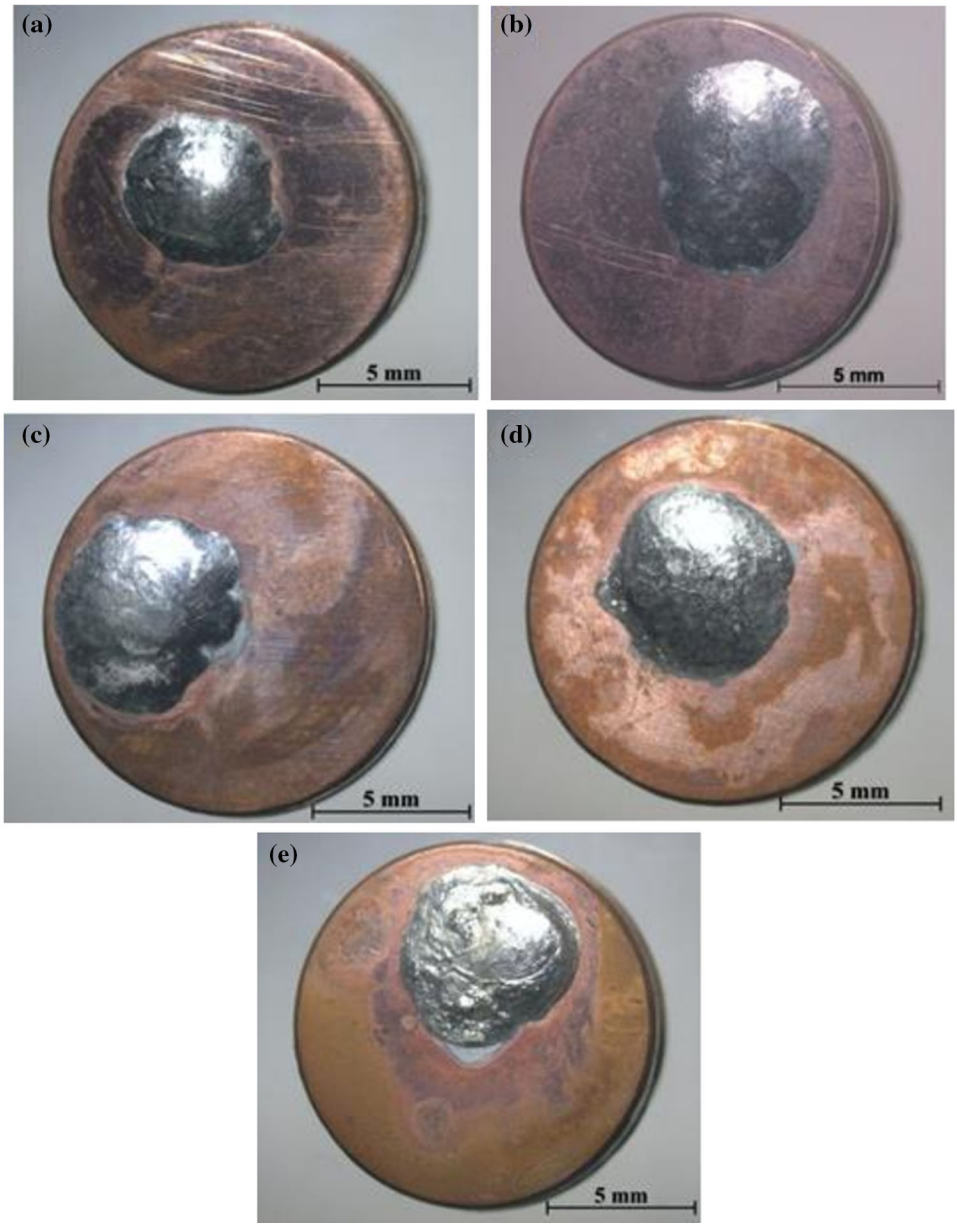

Fig. 5. Macroscopic images (top view) of stabilized Sn-2.5Ag-0.5Cu solder on copper substrate reflowed at 270°C for various times: (a) 10 s, (b) 40 s, (c) 100 s, (d) 300 s, and (e) 500 s.

Sn-2.5Ag-0.5Cu/Cu system were $2.01 \pm 0.76°/s$, $2.68 \pm 0.16°/s$, and $0.02 \pm 0.006°/s$, respectively. Similarly, for the Sn-2.5Ag-0.5Cu/Ni/Cu system, the average relaxation rates in the capillary, gravity, and viscous zones were $0.93 \pm 1.01°/s$, $1.14 \pm 0.18°/s$, and $0.03 \pm 0.002°/s$, respectively. The relaxation rate was higher for Sn-2.5Ag-0.5Cu on bare than Ni-coated Cu substrate in the capillary and gravity zones, whereas comparable relaxation rates were observed in the viscous zone for the two systems. This clearly shows that the wettability of the liquid solder is greater on bare than Ni-coated Cu substrate. A nonuniform relaxation rate was observed in the capillary zone for both the Sn-2.5Ag-0.5Cu/Cu and Sn-2.5Ag-0.5Cu/Ni/Cu systems. This can be attributed to the desire of the molten solder to form a sphere again due to surface tension even though the melting process has started. In this zone, the solder appears to be in a semisolid condition. With the constant supply of heat, the lattice distance between solder atoms further increases, and the solder attains a completely liquid state when the activation energy of solder atoms exceeds the forces between them in the solid state. Therefore, the solder attains a completely liquid state in the gravity zone, and spreading becomes easier. Hence, a higher relaxation rate was observed in the gravity zone compared with the capillary and viscous zones. The stabilized contact angle (θ_f) obtained at the end of the desired reflow time is given in Table II. The

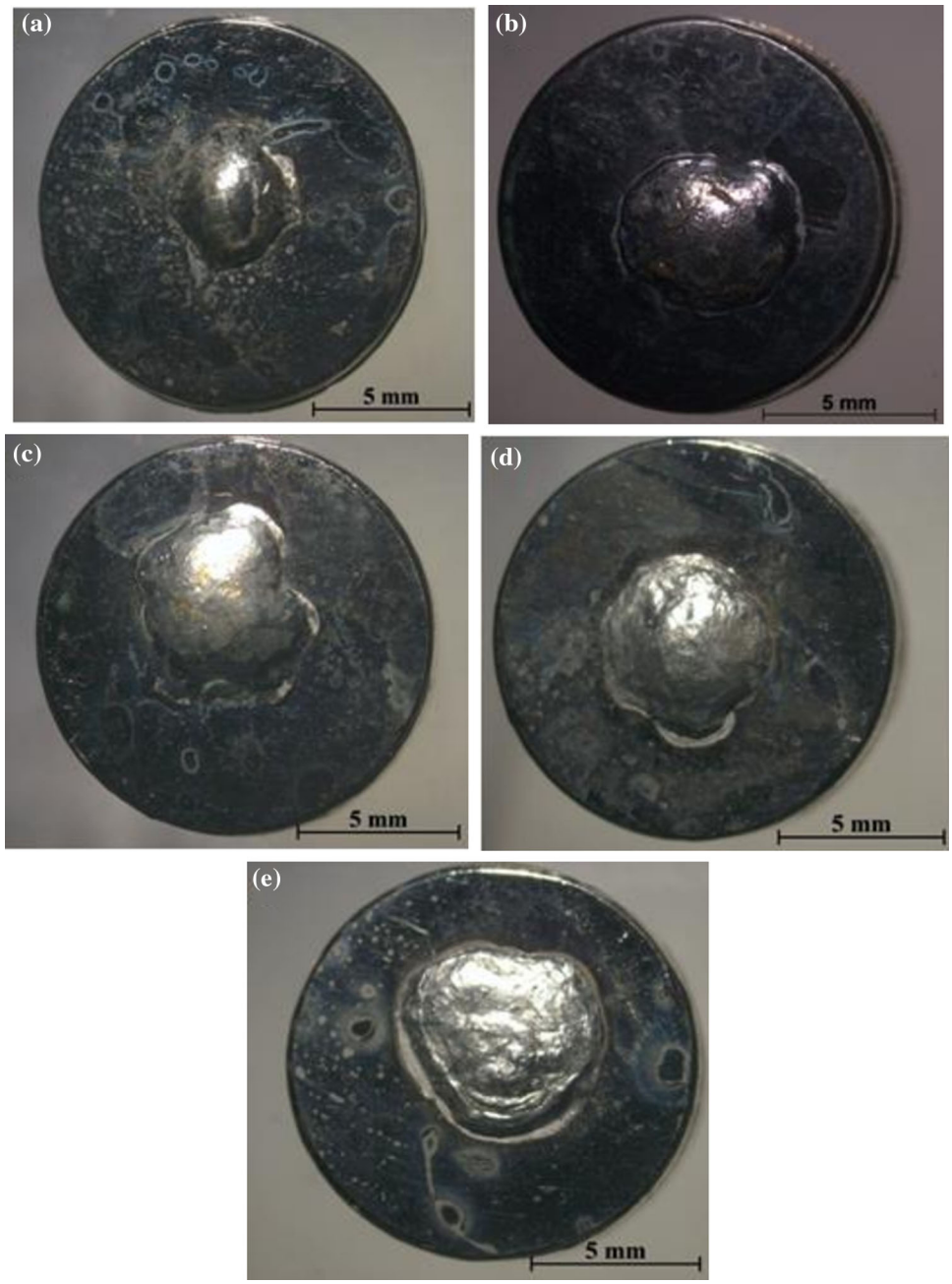

Fig. 6. Macroscopic images (top view) of stabilized Sn-2.5Ag-0.5Cu solder on Ni-coated copper substrate reflowed at 270°C for various times: (a) 10 s, (b) 80 s, (c) 100 s, (d) 300 s, and (e) 500 s.

solder alloy showed enhanced wettability on both bare and Ni-coated Cu substrates at longer reflow times. The stabilized contact angle (θ_f) was lower for Sn-2.5Ag-0.5Cu alloy on bare than Ni-coated Cu substrate for all reflow times. The solder alloy showed good wettability on both substrates for reflow times above 100 s. Figures 5 and 6 show macroscopic images (top view) of stabilized Sn-2.5Ag-0.5Cu droplets on bare and Ni-coated copper substrate, respectively. Reflow time of 10 s was sufficient to melt the solder alloy but insufficient for spreading of solder alloy over the Ni-coated Cu substrate. Therefore, a significant difference in the solder quantity for samples reflowed for 10 s on Ni-coated Cu substrate when compared with other samples can be observed in Fig. 6, although the amount of solder taken was approximately the same in all cases. It can be observed from Figs. 5 and 6 that the spreading area increased with increase of reflow time.

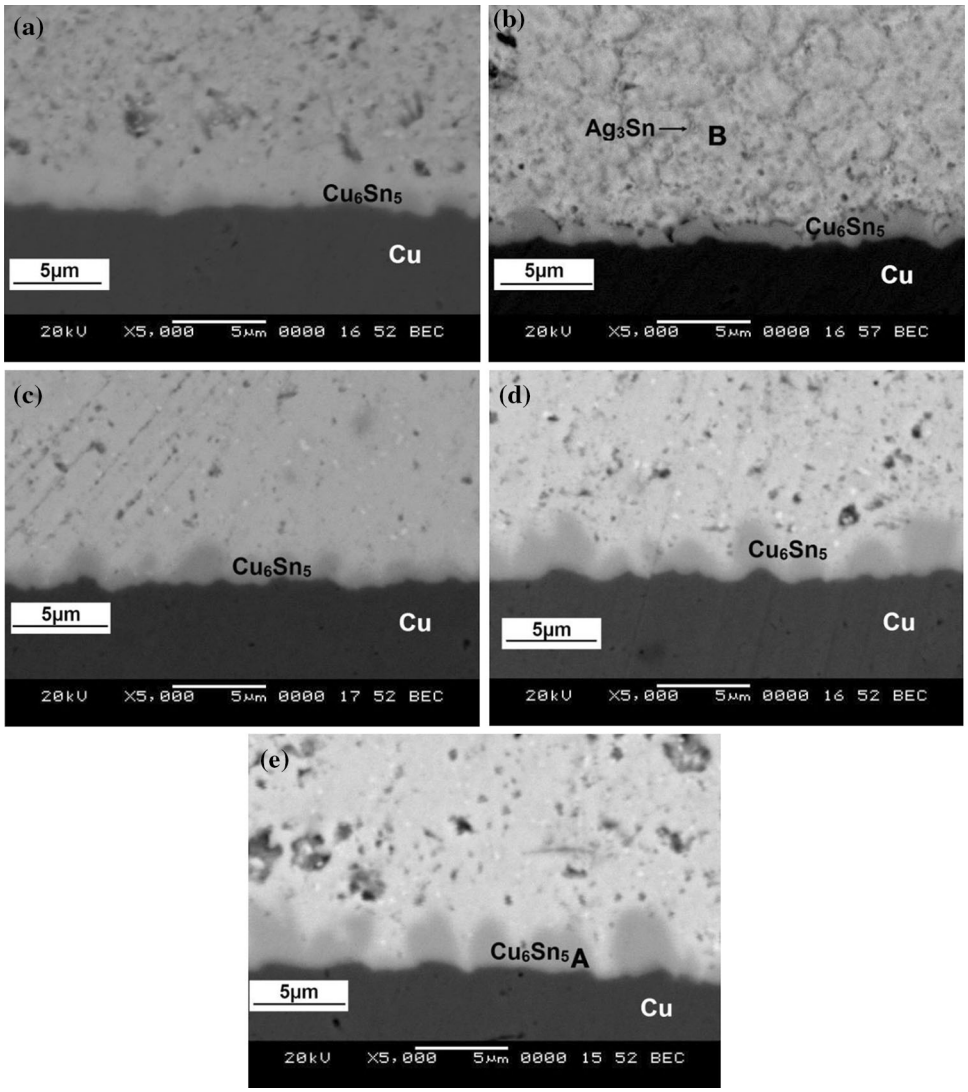

Fig. 7. SEM images of Sn-2.5Ag-0.5Cu/Cu interface reflowed at 270°C for various times: (a) 10 s, (b) 40 s, (c) 100 s, (d) 300 s, and (e) 500 s.

Table III. EDS analysis results of marked regions in Fig. 7 for Sn-2.5Ag-0.5Cu solder on Cu substrate

Mark	Cu K (at.%)	Ag L (at.%)	Sn L (at.%)	Phase
A	51.40	0.44	48.16	Cu_6Sn_5
B	1.03	73.26	25.71	Ag_3Sn

Interfacial Microstructure of Sn-2.5Ag-0.5Cu/Cu and Sn-2.5Ag-0.5Cu/Ni/Cu Joint

The solder drop bonded to the substrate was sectioned along the axis to study the IMC morphology at the interface. Backscattered electron images of the interface were captured to show the boundaries of the interfacial layers more distinctly. Figure 7 shows SEM images of the interface between Sn-2.5Ag-0.5Cu solder alloy and Cu substrate reflowed at 270°C for different reaction times. During the early stage of spreading of the solder alloy, metallic atoms from the Cu substrate that are in contact with the molten solder quickly dissolve into it and become supersaturated at interface regions. Consequently, IMC phases start to nucleate and grow at the interface.[20] The chemical composition of the IMCs revealed that they were composed of Cu and Sn atoms. EDS analysis was carried out to identify the IMCs at the interface. Table III gives the atom percentage of Cu and Sn present in the interfacial region. In all the reaction couples, Cu_6Sn_5 IMC was detected between the solder and

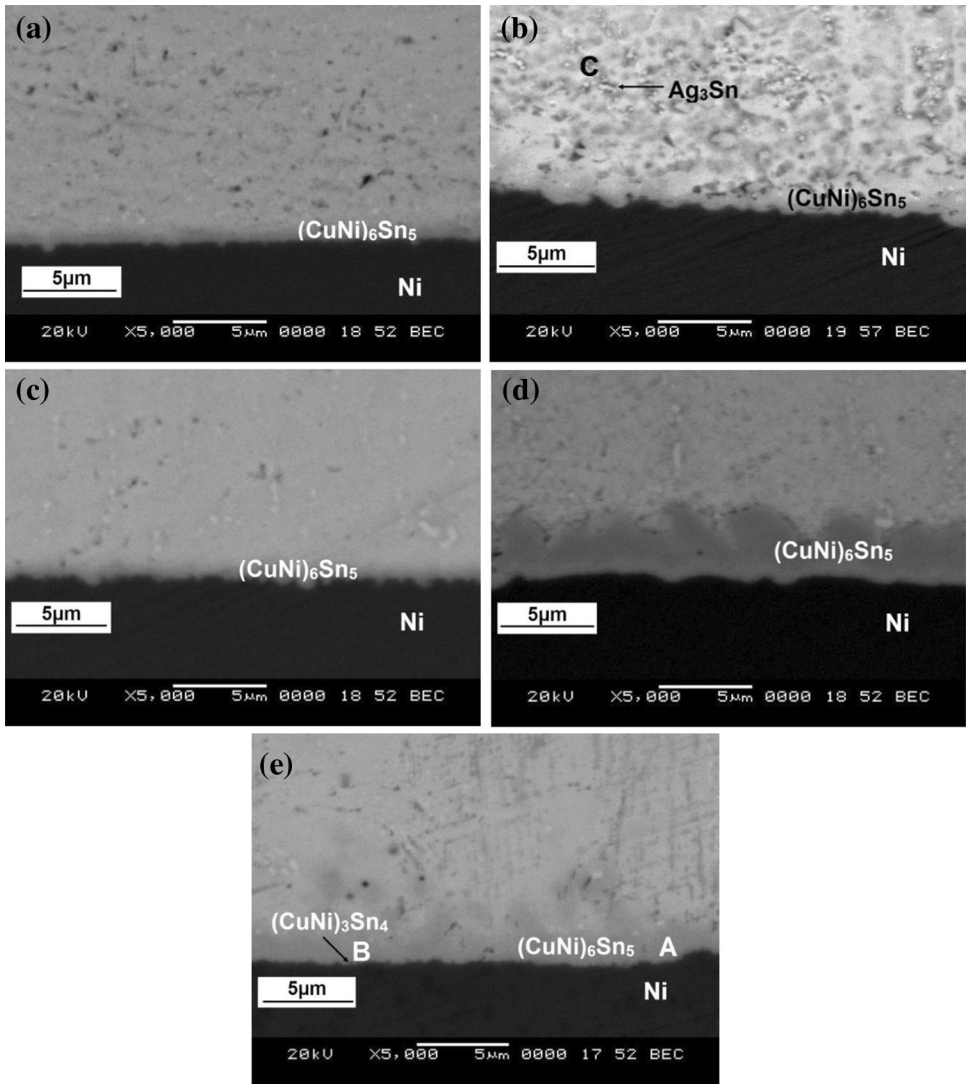

Fig. 8. SEM images of Sn-2.5Ag-0.5Cu/Ni/Cu interface reflowed at 270°C for various times: (a) 10 s, (b) 80 s, (c) 100 s, (d) 300 s, and (e) 500 s.

Table IV. EDS analysis results of marked regions in Fig. 8 for Sn-2.5Ag-0.5Cu solder on Ni-coated Cu substrate

Mark	Cu K (at.%)	Ag L (at.%)	Ni K (at.%)	Sn L (at.%)	Phase
A	30.43	0.34	20.44	48.79	$(CuNi)_6Sn_5$
B	12	0.28	30.62	57.1	$(CuNi)_3Sn_4$
C	1.05	72.57	2.45	23.93	Ag_3Sn

Cu substrate. The rapid coverage of the solder–substrate interface by Cu_6Sn_5 grains gives rise to a continuous Cu_6Sn_5 layer at the interface; the Cu_6Sn_5 grains showed the well-known scallop morphology, being due to the different diffusion rates at the solder–IMC and IMC–Cu interfaces.[7] The thickness of the Cu_6Sn_5 IMC layer increased with increase in reaction time. The IMC thickness was about 0.75 μm for reflow time of 10 s. The IMC thickness was 1.04 μm, 1.197 μm, 1.81 μm, and 1.95 μm for 40 s, 100 s, 300 s, and 500 s, respectively. Greater dissolution of Cu atoms into the molten solder during longer reflow time intervals is the main reason for the increase in the IMC thickness at longer reaction times. The presence of Ag_3Sn precipitates was also detected in the matrix

region of the solder. However, Ag_3Sn IMC was not uniformly distributed but was precipitated only at a few locations in the solder matrix.

Figure 8 shows SEM images (backscattered electron mode) of the interface between Sn-2.5Ag-0.5Cu solder and Ni-coated Cu substrate reflowed at 270°C for various reaction times. The chemical composition of the IMCs revealed that they were composed of Cu, Ni, and Sn atoms. $(Cu,Ni)_6Sn_5$ and $(Cu,Ni)_3Sn_4$ were the two kinds of reaction products identified at the interface. Table IV gives the atom percentage of Cu, Ni, and Sn present in the interfacial region. $(Cu,Ni)_6Sn_5$ IMC was solely found at the solder–substrate interface up to reflow time of 300 s, showing scallop morphology. Cu from the solder combined with Ni and Sn to form $(Cu,Ni)_6Sn_5$ IMC. The thickness of the $(Cu,Ni)_6Sn_5$ IMC was found to increase up to reflow time of 300 s. The IMC thickness was 0.69 μm, 0.84 μm, 1.81 μm, and 2.86 μm for reflow time of 10 s, 80 s, 100 s, and 300 s, respectively. Eventually, this growing phase consumes essentially all the available Cu in the solder. After Cu has been essentially consumed from the Sn-Ag-Cu bulk solder, $(Cu,Ni)_6Sn_5$ is eventually replaced by $(Cu,Ni)_3Sn_4$.[21,22] Both $(Cu,Ni)_6Sn_5$ and $(Cu,Ni)_3Sn_4$ IMCs were found in samples reflowed for 500 s. The thickness of the $(Cu,Ni)_6Sn_5$ IMC dropped to 1.99 μm for reflow time of 500 s. This reduction in thickness of $(Cu,Ni)_6Sn_5$ observed for samples reflowed for 500 s was attributed to the decrease of the available Cu in the solder bulk matrix.

The thickness of the IMCs formed at the interface was lower on the Ni-coated Cu substrate compared with the bare Cu substrate up to reflow time of 100 s. This clearly indicates that Ni acts as a diffusion barrier to prevent rapid reaction of the molten solder with the Cu substrate. The IMC thickness was found to be greater at the interface of Sn-2.5Ag-0.5Cu solder and Ni-coated Cu substrate for longer reflow times. The growth kinetics of the IMC layer was studied. The obtained thickness values were fit according to the growth model

$$y = kt^n, \quad (1)$$

where y is the intermetallic layer thickness, k is the growth constant, t is the reflow time, and n is the growth exponent. If the growth exponent (n) is equal to 1/3, it is assumed that the growth of the IMC layer is dominated by grain-boundary (GB) diffusion and limited by coarsening of the microstructure.[7,23] Therefore, the curve was force fit with a value of the exponent (n) equal to 1/3. The obtained adj. R^2 values were 0.93 and 0.62 for the Sn-2.5Ag-0.5Cu/Cu and Sn-2.5Ag-0.5Cu/Ni/Cu system, respectively. This shows that GB diffusion is the primary transport mechanism contributing to the rate-controlling process for IMC growth in both the Sn-2.5Ag-0.5Cu/Cu and Sn-2.5Ag-0.5Cu/Ni/Cu systems. A plot of IMC thickness versus reflow time for Sn-2.5Ag-0.5Cu solder alloy on bare and Ni-coated Cu substrates is shown in Fig. 9.

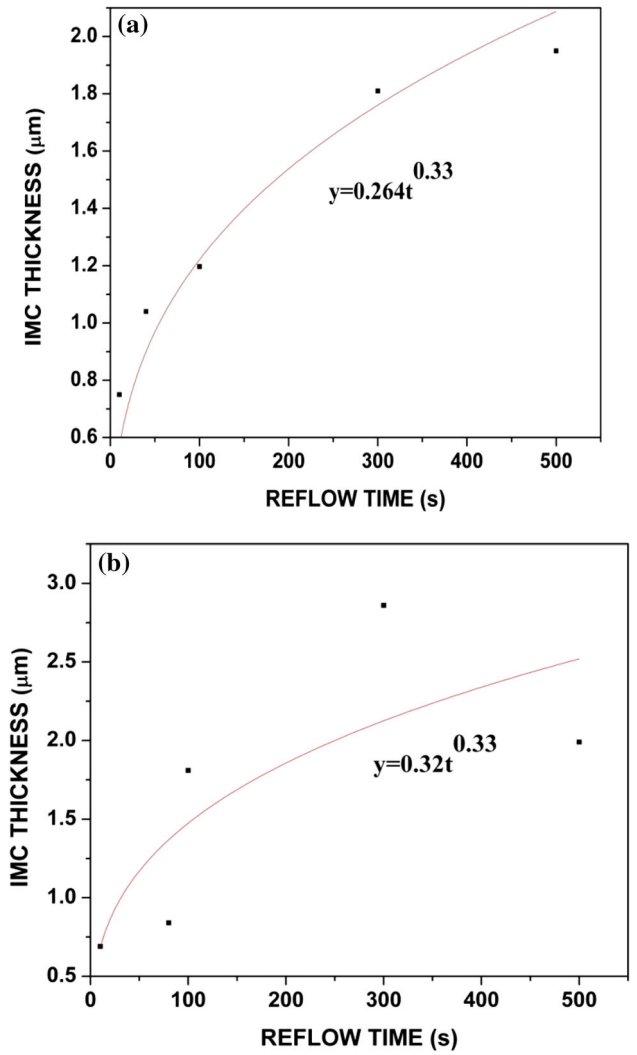

Fig. 9. IMC thickness versus reflow time for Sn-2.5Ag-0.5Cu solder alloy on (a) bare and (b) Ni-coated Cu substrate.

Shear Strength of Sn-2.5Ag-0.5Cu/Cu and Sn-2.5Ag-0.5Cu/Ni/Cu Joint

Ball shear testing was performed to evaluate the effect of the interfacial reactions on the bond strength as a function of reflow time. Figures 10 and 11 show force–distance curves obtained during shear tests for the Sn-2.5Ag-0.5Cu/Cu and Sn-2.5Ag-0.5Cu/Ni/Cu system, respectively. Three sets of experiments were carried out to obtain consistent results, and the error bars on the force–distance curves indicate the standard deviation in the shear strength values in these three sets of tests. The variation in the spread area of the sessile drop resulted in slight scatter in the force–distance curves. The shear energy values are given in Table V. The force–distance curves exhibited a

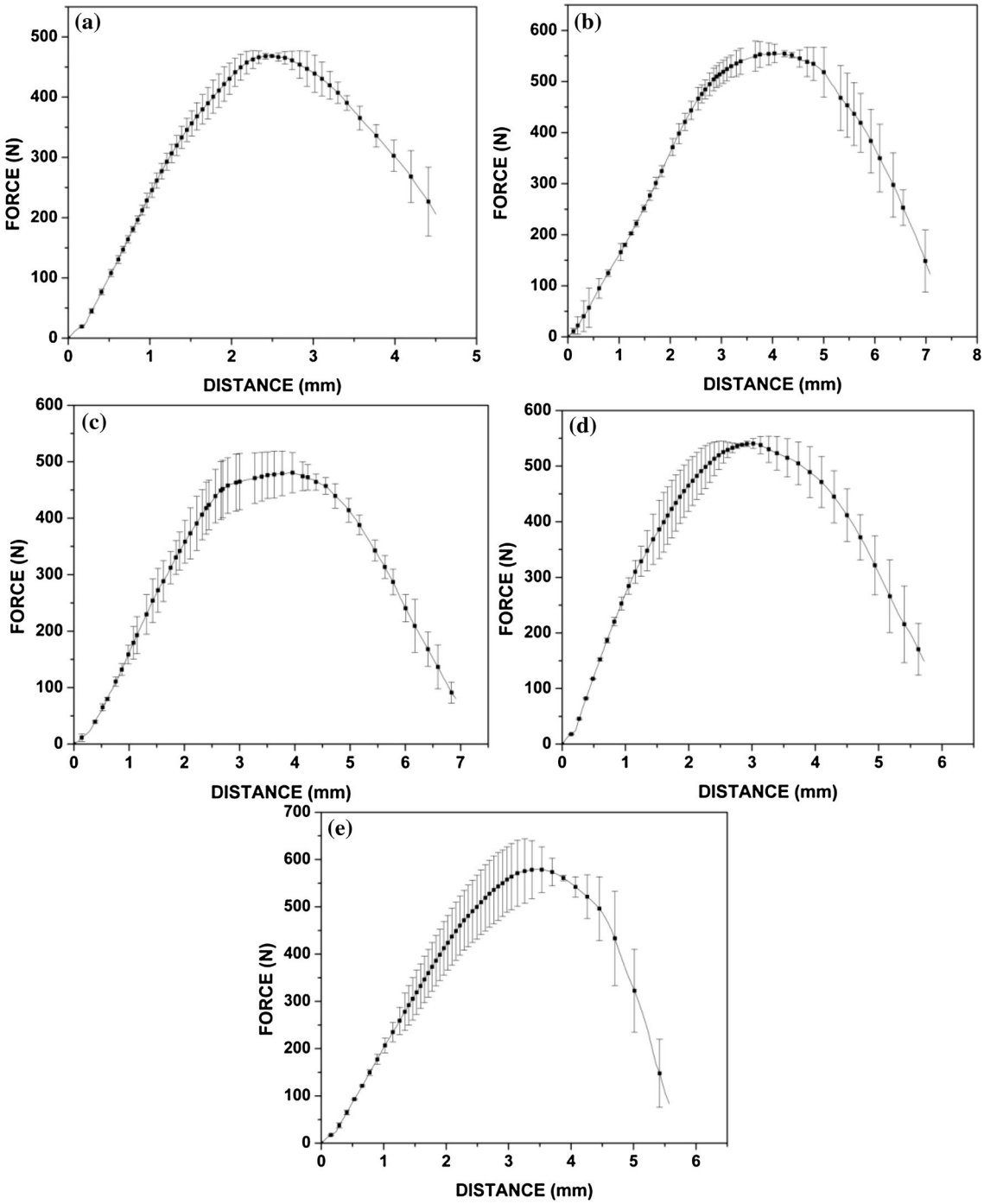

Fig. 10. Shear force–distance curves for Sn-2.5Ag-0.5Cu solder reflowed on copper substrate for various times: (a) 10 s, (b) 40 s, (c) 100 s, (d) 300 s, and (e) 500 s.

gradual decrease after reaching a peak value. The Sn-2.5Ag-0.5Cu/Cu system showed maximum bond strength for reflow time of 40 s, whereas the Sn-2.5Ag-0.5Cu/Ni/Cu system showed maximum bond strength for reflow time of 80 s. Since 40 s and 80 s are the approximate times at which the gravity zone comes to an end in both the Sn-2.5Ag-0.5Cu/Cu and Sn-2.5Ag-0.5Cu/Ni/Cu systems, we concluded that the dynamic contact angle at the end of the gravity zone (θ_{gz}) is responsible for the maximum bond strength. Bond strength decreased with further increase in reflow time and IMC thickness in later stages. This also suggests that solder reflow should not extend beyond the gravity regime.

The Sn-2.5Ag-0.5Cu/Ni/Cu system showed the maximum bond strength among the two systems for

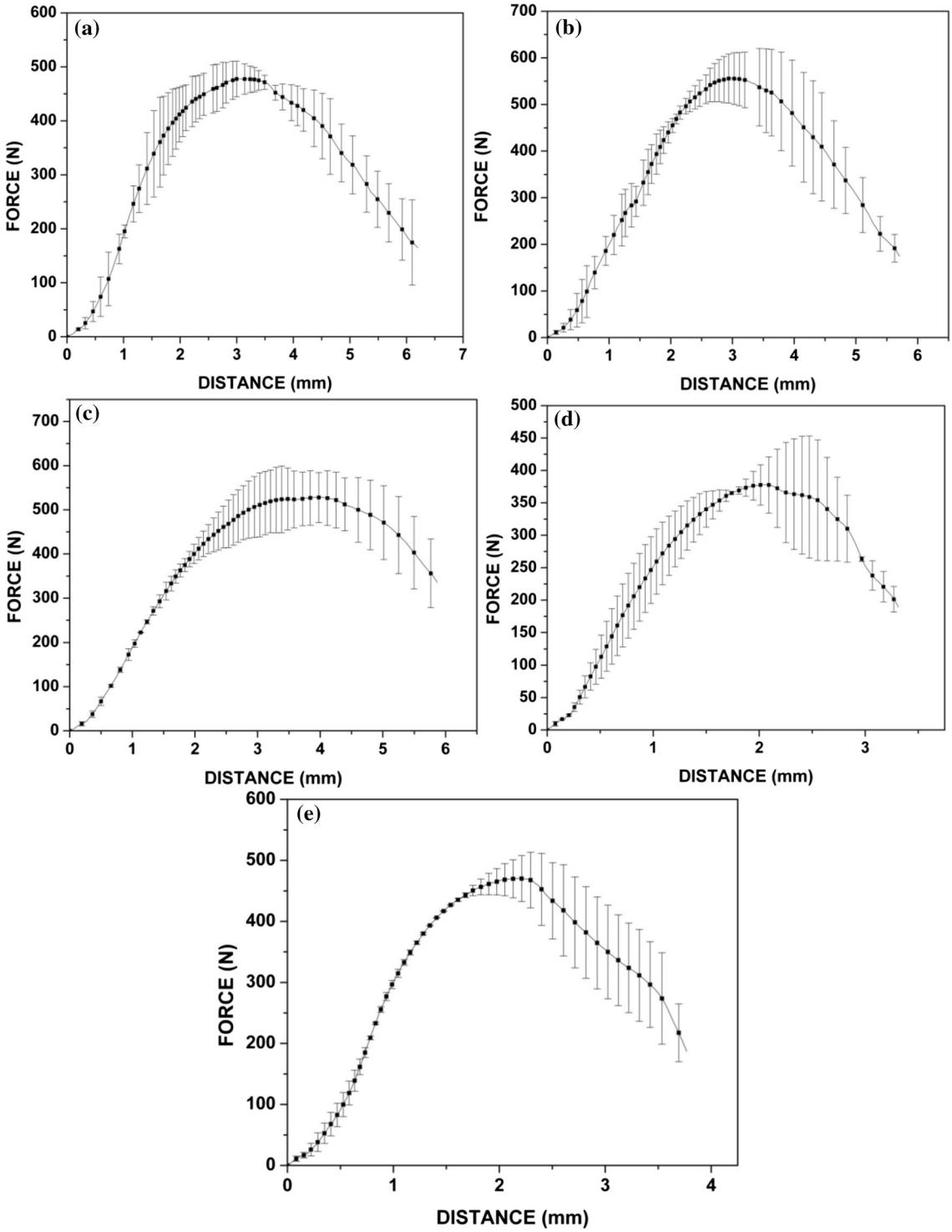

Fig. 11. Shear force–distance curves for Sn-2.5Ag-0.5Cu solder reflowed on Ni-coated copper substrate for various times: (a) 10 s, (b) 80 s, (c) 100 s, (d) 300 s, and (e) 500 s.

various reflow times. There is a large variation in the mechanical properties of the $(Cu,Ni)_6Sn_5$ and Cu_6Sn_5 IMCs due to their anisotropic mechanical properties combined with their different crystal orientations. Use of Ni in solder alloys or as substrate has many beneficial effects on the $(Cu,Ni)_6Sn_5$ IMC layer, such as stabilization of the hexagonal phase to room temperature, effective reduction of thermal stress of solder joints, reduced anisotropy of mechanical behavior, improved mechanical behavior including increased creep stress exponent, and lower propensity for crack formation.[24–27]

Table V. Shear energy of Sn-2.5Ag-0.5Cu solder alloy reflowed on bare and Ni-coated Cu substrate

Sn-2.5Ag-0.5Cu/Cu		Sn-2.5Ag-0.5Cu/Ni/Cu	
Reflow time (s)	**Shear energy (kJ/m^2)**	**Reflow time (s)**	**Shear energy (kJ/m^2)**
10	67 ± 1.58	10	69.71 ± 0.41
40	91.39 ± 3.40	80	97.4 ± 4.2
100	74.98 ± 0.37	100	79.38 ± 0.99
300	77.67 ± 2.01	300	56.91 ± 0.59
500	67.01 ± 2.14	500	63.74 ± 2.05

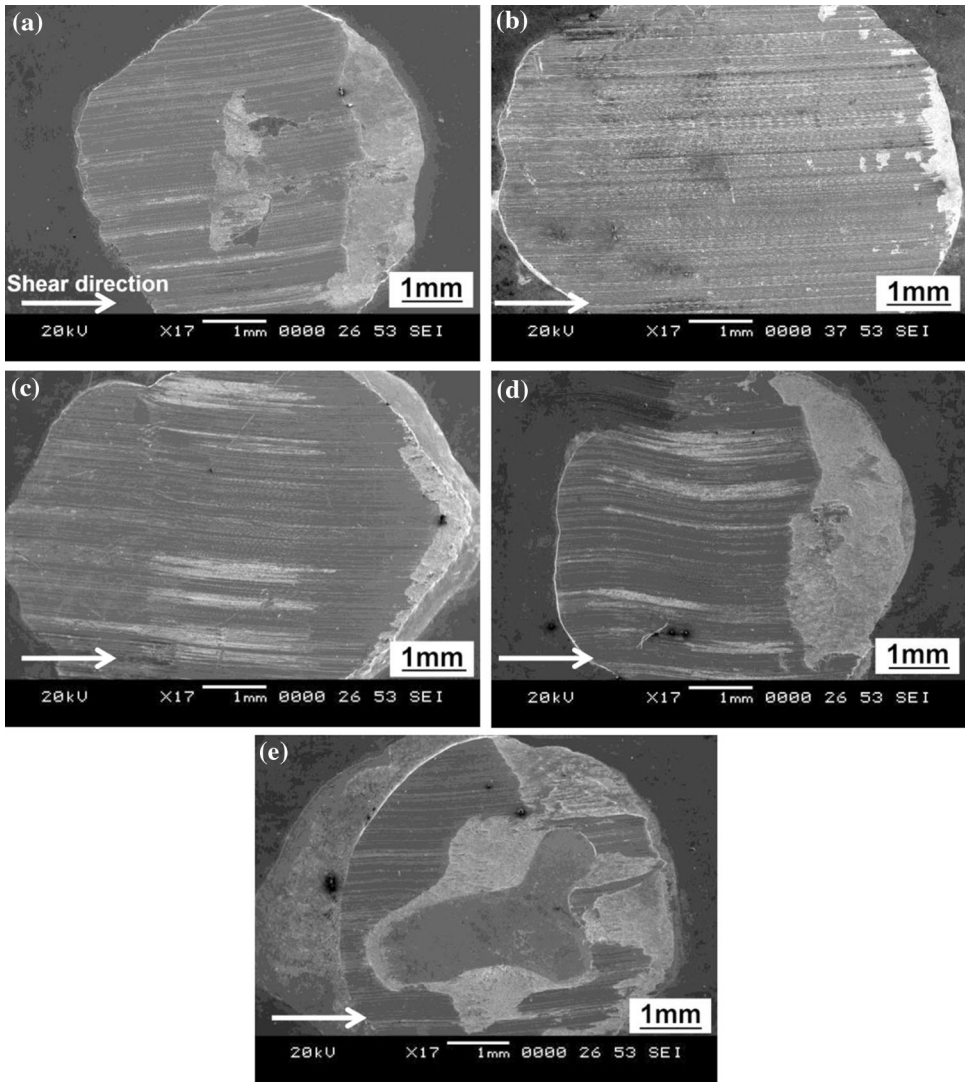

Fig. 12. SEM images of fractured surfaces of Sn-2.5Ag-0.5Cu/Cu reflowed for (a) 10 s, (b) 40 s, (c) 100 s, (d) 300 s, and (e) 500 s.

Fractured surfaces were observed under scanning electron microscopy to study the failure mode of the joints. Fractured surfaces are shown in Figs. 12 and 13 for the Sn-2.5Ag-0.5Cu/Cu and Sn-2.5Ag-0.5Cu/Ni/Cu system, respectively, where arrows indicate the shear direction. EDS analysis on the fractured surfaces indicated the occurrence of failure predominantly in bulk solder regardless of reflow time. However, a transition ridge was seen on all samples at the edge (right side) of the solder–substrate system where the shear tool stopped its motion during the shear test. This is due to backstress

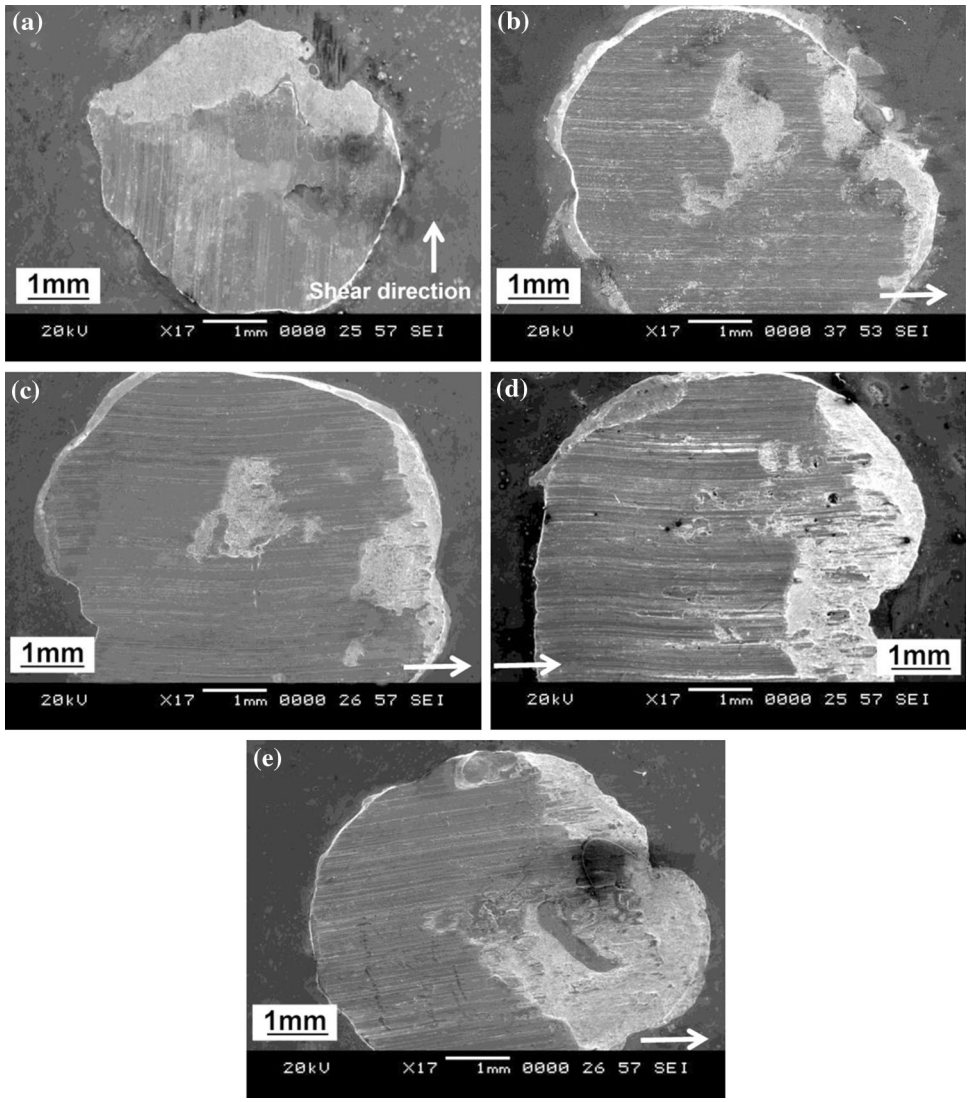

Fig. 13. SEM images of fractured surfaces of Sn-2.5Ag-0.5Cu/Ni/Cu reflowed for (a) 10 s, (b) 80 s, (c) 100 s, (d) 300 s, and (e) 500 s.

gradually developed by work hardening, which restricts the deformation of the solder alloy during the shear test. Therefore, higher stresses are concentrated at the transition ridge. The presence of such a transition ridge on the fractured surfaces indicates that the shear tool moved from the bulk to the interfacial region. All the solder–substrate systems exhibited ductile fracture in the bulk region, whereas brittle fracture was observed in the interfacial region.

CONCLUSIONS

Based on study of the effect of reflow time on wettability and interfacial reactions of Sn-2.5Ag-0.5Cu solder alloy on bare and Ni-coated Cu substrates, the following conclusions can be drawn:

1. Both the Sn-2.5Ag-0.5Cu/Cu and Sn-2.5Ag-0.5Cu/Ni/Cu systems showed good wettability for longer reflow times. The spreading behavior of the solder alloy was characterized into capillary, gravity (diffusion), and viscous zones.
2. The gravity (diffusion) zone was obtained from 3.8 ± 0.43 s to 38.97 ± 3.38 s and 5.99 ± 0.5 s to 77.82 ± 8.84 s for the Sn-2.5Ag-0.5Cu/Cu and Sn-2.5Ag-0.5Cu/Ni/Cu system, respectively.
3. Sn-2.5Ag-0.5Cu solder reflowed for 40 s on Cu substrate and 80 s on Ni-coated Cu substrate yielded the maximum joint strength compared with that obtained for reflow times required to achieve stabilized contact angle (θ_f). The Sn-2.5Ag-0.5Cu/Ni/Cu system reflowed for 80 s showed maximum bond strength among both solder–substrate systems reflowed for various times.
4. Sn-2.5Ag-0.5Cu solder alloy reflowed on Cu substrate for various reflow times showed

Cu_6Sn_5 intermetallic at the interface irrespective of the reflow time. The thickness of Cu_6Sn_5 IMC increased with increase in reflow time. Similarly, the Sn-2.5Ag-0.5Cu/Ni/Cu system showed $(Cu,Ni)_6Sn_5$ intermetallic at the interface; its thickness increased up to 300 s, followed by a decrease thereafter. The samples reflowed for 500 s showed spalling, resulting in decreased joint strength.

5. Grain-boundary diffusion was found to be the rate-controlling process for IMC growth in both the Sn-2.5Ag-0.5Cu/Cu and Sn-2.5Ag-0.5Cu/Ni/Cu systems.
6. The thickness of IMCs formed at the interface was lower on Ni-coated compared with bare Cu substrate up to reflow time of 100 s, whereas the IMC thickness was found to be greater at the interface of Sn-2.5Ag-0.5Cu solder and Ni-coated Cu substrate for longer reflow times.
7. IMC thickness between 1 μm and 1.81 μm gave higher joint strength for the Sn-2.5Ag-0.5Cu/Cu and Sn-2.5Ag-0.5Cu/Ni/Cu systems.
8. A transition ridge was seen on all fractured surfaces, indicating that the shear tool moved from the bulk to interfacial region.
9. A dynamic contact angle (θ_g) was found to be a better parameter compared with the stabilized contact angle (θ_f) in correlating the wettability of liquid solder to the microstructure and joint strength. The study suggests that solder reflow should end before the start of the viscous regime, clearly highlighting the importance of the gravity zone in determining the optimum reflow time for lead-free solder alloys.

ACKNOWLEDGEMENTS

The authors thank the Defence Research Development Organization (DRDO), Govt. of India, New Delhi for financial support under Research Grant ERIP/ER/1006009M/01/1356.

REFERENCES

1. H. Tsukamoto, T. Nishimura, S. Suenaga, and K. Nogita, *Mater. Sci. Eng. B* 171, 162 (2010).
2. D.Q. Yu, J. Zhao, and L. Wang, *J. Alloys Compd.* 376, 170 (2004).
3. C.Y. Ho and J.G. Duh, *Mater. Lett.* 92, 278 (2013).
4. Satyanarayan and K.N. Prabhu, *Adv. Colloid Interface Sci.* 166, 87 (2011).
5. B.L. Silva, N. Cheung, A. Garcia, and J.E. Spinelli, *Mater. Lett.* 142, 163 (2015).
6. M. Arra, D. Shangguan, E. Ristolainen, and T. Lepisto, *Solder Surf. Mt. Tech.* 14, 18 (2002).
7. M.S. Park, M.K. Stephenson, C. Shannon, L.A.C. Diaz, K.A. Hudspeth, S.L. Gibbons, M.J. Saldana, and R. Arroyave, *Acta Mater.* 60, 5125 (2012).
8. M. Sona and K.N. Prabhu, *Trans. Indian Inst. Met.* (2015). doi:10.1007/s12666-015-0590-0.
9. S. Amore, E. Ricci, G. Borzone, and R. Novakovic, *Mater. Sci. Eng. A* 495, 108 (2008).
10. M. Sona and K.N. Prabhu, *J. Mater. Sci. Mater. El.* 24, 3149 (2013).
11. A. Choubey, H. Yu, M. Osterman, M. Pecht, F. Yun, L. Yonghong, and X. Ming, *J. Electron. Mater.* 37, 1130 (2008).
12. A.A.E. Daly and A.M.E. Taher, *Mater. Des.* 47, 607 (2013).
13. T. Laurila and V. Vuorinen, *Materials* 2, 1796 (2009).
14. D. Mu, H. Huang, and K. Nogita, *Mater. Lett.* 86, 46 (2012).
15. J. Pan, J. Wang, and D.M. Shaddock, *Proceedings of the 37th International Symposium on Microelectronics*, (2004).
16. M.N. Islam, Y.C. Chan, A. Sharif, and M.O. Alam, *Microelectron. Reliab.* 43, 2031 (2003).
17. T. You, Y. Kim, W. Jung, J. Moon, and H. Choe, *J. Alloys Compd.* 486, 242 (2009).
18. C.M. Chen and H.C. Lin, *J. Electron. Mater.* 35, 1937 (2006).
19. M. Sona and K.N. Prabhu, *SMTA J.* 28, 36 (2015).
20. Z. Dariavach, P. Callahan, J. Liang, and R. Fournelle, *J. Electron. Mater.* 35, 1581 (2006).
21. C.K. Wong, J.H.L. Pang, J.W. Tew, B.K. Lok, H.J. Lu, F.L. Ng, and Y.F. Sun, *Microelectron. Reliab.* 48, 611 (2008).
22. A. Zribi, A. Clark, L. Zavalij, P. Borgesen, and E.J. Cotts, *J. Electron. Mater.* 30, 1157 (2001).
23. M. Schaefer, R. Fournelle, and J. Liang, *J. Electron. Mater.* 27, 1167 (1998).
24. J.M. Song, C.W. Su, Y.S. Lai, and Y.T. Chiu, *J. Mater. Res.* 25, 629 (2010).
25. Q.K. Zhang, J. Tan, and Z.F. Zhang, *J. Appl. Phys.* 110, 014502 (2011).
26. D. Mu, H. Yasuda, H. Huang, and K. Nogita, *J. Alloys Compd.* 536, 38 (2012).
27. D. Mu, H. Huang, S.D. McDonald, J. Read, and K. Nogita, *Mater. Sci. Eng. A* 566, 126 (2013).